PERGAMON

Carbon 41 (2003) 1625–1634

CARBON

Mechanism for the growth of multiwalled carbon-nanotubes from carbon black

D.B. Buchholz, S.P. Doherty, R.P.H. Chang*

Department of Materials Science and Engineering, Northwestern University, 2220 Campus Dr., Room 2011, Evanston, IL 60208, USA

Received 21 February 2003; received in revised form 3 March 2003; accepted 4 March 2003

Abstract

Multiwalled carbon-nanotubes have been grown from carbon black by solid-state transformation at the anode of a modified high-temperature arc-furnace without a catalyst. A mechanism for the solid-state transformation of carbon black into nanotubes is proposed. The migration of pentagon and heptagon defects present in carbon black to regions of high tensile-stress is key to the growth mechanism. The growth process can be broken into two stages. The basic mechanism for both stages is the same; only the source of the tensile stress that drives the nanotube growth differs. In the initial stage of growth the necks between carbon-black particles are lengthened into short nanotubes by thermal forces. Electrostatic forces present in the plasma of the high-temperature arc-furnace drive the subsequent extension of the short nanotubes to multiple-micron lengths.

Keywords: A. Carbon black, Carbon nanotubes; B. Arc discharge

1. Introduction

Large-scale production of carbon nanotubes is necessary for nanotubes to reach their full technological-potential. A key to production scale-up is an understanding of the mechanism by which the nanotubes are formed. Naturally, the particulars of a growth mechanism will depend on the method used to grow the material. Recently, we reported on the growth of multiwalled carbon-nanotubes (MWNTs) from carbon black by heating in a high-temperature arc-furnace [1]. In this earlier work, carbon black was determined to be the source of carbon for the growth of MWNTs and a growth-mechanism outlined. In this paper we provide a detailed explanation of the solid-state growth-mechanism by which carbon black is transformed into MWNTs.

Considerable work has been done with regard to investigating the growth of carbon nanotubes from the vapor phase [2]. It is recognized, however, that given the appropriate conditions, solid-state formation of carbon precursor materials to fullerene-related particles [3,4] short tube-like structures [5,6] and carbon nanotubes is possible [7,8]. Additionally, for some types of nanotube growth, even when the carbon necessary for the growth of the nanotube is transported to the growth region in the vapor phase, the actual growth-mechanism is proposed to be by solid-state diffusion and root growth [9,10]. The proposed solid-state processes include: one, a proper growth site; and two, a sufficiently high temperature to facilitate solid-state transport. In the system under study in this paper, carbon black provides the proper growth sites and an arc furnace is used to achieve the temperatures necessary for rapid solid-state diffusion.

A key element to the mechanism proposed is defects in the carbon-black graphene-layers. Pentagon and heptagon rings are two types of defects found in graphene layers. The introduction of pentagons, heptagons and pentagon–heptagon pairs [11] into a graphene layer modifies the topology of the structure. The insertion of a pentagon into a hexagonal network introduces positive curvature to the graphene structure [12] and is the means by which carbon nano-cones are formed [13], carbon nanotubes are capped [14,15], and fullerenes form closed structures [16]. The insertion of a heptagon into a hexagonal network introduces negative curvature to the graphene structure [17,18] and is used to explain the branching of nanotubes into T, Y

*Corresponding author. Tel.: +1-847-491-3598; fax: +1-847-491-4181.

E-mail address: r-chang@northwestern.edu (R.P.H. Chang).

0008-6223/03/$ – see front matter
doi:10.1016/S0008-6223(03)00110-6

and X junctions [19,20] as well as leading to the speculation of negatively curved analogs to fullerenes [21,22]. Although the insertion of a pentagon–heptagon pair into a hexagonal network introduces no net curvature the pair results in many topological features [23]. Pentagon–heptagon pairs are the means by which fullerene polyhedra obtain a more spherical-form [24,25], junctions are formed between carbon nanotubes of different chirality [26,27], tapers are formed in carbon nanotubes [17,28], and is proposed as a mechanism by which strain is released from carbon-nanotubes loaded in tension [29].

Prior to the discovery of fullerenes the existence of pentagons or heptagons as a defect in the graphene structure of carbon black was not considered [30]. Structures, other than those that contained 120° angles had to be explained in terms of sp^3 bonding [31]. When it was discovered that fullerenes and carbon black could be produced in similar processes, it was concluded that fullerene-like structures could be present in carbon black [32,33]. High-resolution electron microscopy has established the existence of fullerene like structures both in the bulk and on the surface of carbon-black particles [34]. A current model of carbon black is that of an aggregate of semi-spherical carbon-onion like structures, built up by concentric carbon-layers around a defect-fullerene nucleus [35] (see Fig. 1a). The onion like structures are joined in an aggregate by multiple carbon-layers that encase several onion structures (see Fig. 1b). This structure requires a large number of pentagon and heptagon defects to be present in the graphene lattice. The endohedral nature of the onion like structures requires pentagons to exist in the graphitic network. The spherical, as opposed to polyhedral, topology of the onion like structures would require the presence of pentagon–heptagon pair defects, which will be noted as [5–7] defects from this point on. The negative curvature in the graphitic over-layers at the point of tangency between carbon-onions (necks) would require heptagons in the graphitic network, as indicated by the arrow in Fig. 1b. The pentagon, heptagon and [5–7] defects are the key that allows solid-state transformation of carbon black into MWNTs at the anode of the high-temperature arc-furnace, and why materials such as graphite, which lack these defects, do not undergo the same transformation.

The electric field generated by the bias between the electrodes of the arc furnace, and augmented by the electric field resulting from the plasma sheath, is believed to play a second key-role in achieving the long tube-lengths observed in the solid-state growth from carbon black. Although nanotubes have also been grown by solid-state transformation, the best efforts to date, in the absence of an electric field, are on the order of 1 μm in length [36]. For the solid-state transformation of carbon black at the anode of a high-temperature arc-furnace the nanotubes are frequently on the order of 100 μm in length (see Fig. 2).

Electric fields have been observed to have a large effect on carbon nanotubes. For carbon nanotubes grown by microwave plasma-enhanced chemical vapor deposition, the aligned growth of the nanotubes is attributed to the electric field generated by the plasma-sheath self-bias (~0.1 V μm^{-1}) [37]. Post growth-process alignment of carbon-nanotubes grown by the carbon-arc method, has been reported when a relatively weak electric-field (~0.2

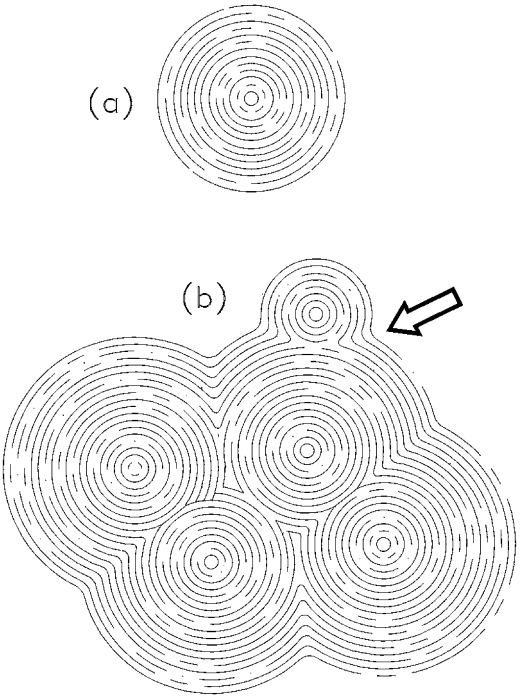

Fig. 1. Schematic representation of carbon black. (a) Carbon-onion like structure; (b) aggregate of carbon-onion like structures (arrow indicates ‘neck’ between carbon-onions).

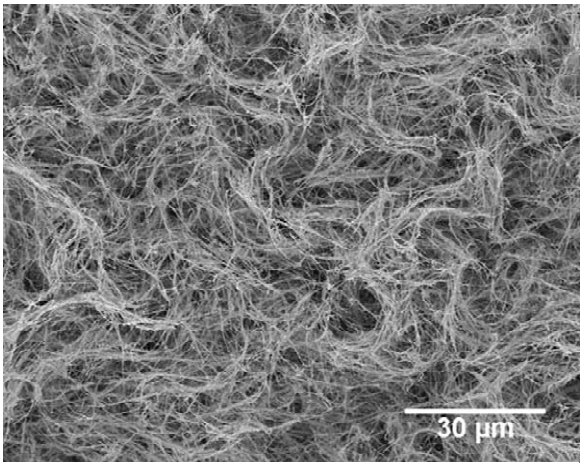

Fig. 2. Typical multi-micron long MWNTs.

V μm^{-1}) is applied, in situ, immediately after the growth process [38]. Slightly stronger, but still rather modest, electric fields (10–100 V μm^{-1} as estimated from micrographs in the following references) have been used to straighten curved nanotubes [39] and bend straight nanotubes [40] by as much as 80°.

The force of the electric field on a carbon nanotube can be estimate from first principles. The electric force, $\boldsymbol{F}$, on a point charge, q_o, in an electric field, $\boldsymbol{E}$, is defined as $\boldsymbol{F} = \boldsymbol{E}q_o$ and for a general distribution of charge as $\boldsymbol{F} = \int \boldsymbol{E}\, dq$. If $\boldsymbol{E}$ is constant:

$$\boldsymbol{F} = Q\boldsymbol{E} \tag{1}$$

where Q is the general charge-distribution in a constant $\boldsymbol{E}$-field. Recognizing that a stress, σ_s, is a force per unit area:

$$\sigma_s = \boldsymbol{F}/A \tag{2}$$

and that the surface charge-density, σ_q, is the general charge-distribution per unit area:

$$\sigma_q = Q/A \tag{3}$$

Eq. (1) can be rewritten in terms of stress and charge density:

$$\sigma_s = \sigma_q \boldsymbol{E} \tag{4}$$

The charge distribution in the nanotube can be estimated from first principles assuming the nanotube to be a conductor. For a conductor immersed in a static field, Gauss's law requires the field within a conductor to be zero and the field at the surface to be normal, $\boldsymbol{n}$, to the conductor. To achieve the zero-field condition, the electrons within the conductor redistribute themselves such that the charge density at the surface, σ_q, exactly balances the external electric-field:

$$\boldsymbol{E} = (\sigma_q/\varepsilon_o)\,\boldsymbol{n} \quad \text{or} \quad \sigma_q = \varepsilon_o \boldsymbol{E} \tag{5}$$

where ε_o is the electric permittivity. The surface charge-density of Eq. (5) can be substituted into Eq. (4) to yield an expression for the stress experienced by a nanotube that depends only on the electric-field strength at the surface of the tube:

$$\sigma_s = \varepsilon_o \boldsymbol{E}^2 \tag{6}$$

The electric field experienced by the tip of a nanotube, $\boldsymbol{E}_{tip}$, will not be the same as that experienced by a planer-object subjected to the same ambient field, $\boldsymbol{E}_{amb}$. The long thin geometry of the nanotube enhances the electric field experienced at the tip. The enhancement to the electric field at the tip of a single-walled nanotube has been calculated by Maiti et al. [41]. For closed tips, the field at the tip is enhanced by a factor of:

$$\boldsymbol{E}_{tip} = \boldsymbol{E}_{amb} \cdot [0.87(L/R) + 4.5] \tag{7}$$

where R and L are the radius and length of the tube, respectively, and is valid for the range 0.2 nm$<R<$10 nm, 20 nm$<L<$60 nm and $L/R>5$.

Although Eq. (7) is not directly applicable to MWNTs, it will be used to estimate the order-of-magnitude affect the nanotube geometry has on the electric field. For a short nanotube, $L/R=10$, the electric field is enhanced by a factor of 13, $\boldsymbol{E}_{tip}/\boldsymbol{E}_{amb} = 13$, and because the stress induced on the nanotube is dependent on the square of the electric field the stress is enhanced by a factor of 175. For $L/R=50$ the stress induced by the electric field is enhanced by a factor of 2300. What is clear from Eqs. (6) and (7) is that once started, an electric-field assisted growth-mechanism will accelerate the rate of tube growth the longer a tube becomes.

2. Experimental

The system in which the MWNTs are formed has been described extensively elsewhere [42]. Basically, it is a two-electrode, DC, high-temperature arc-furnace. The cathode is a solid, flat-faced, 3/8″ diameter rod of randomly oriented graphite (ROG). The anode, where the MWNTs are formed, is fabricated from a 3/8″ diameter ROG rod. A hole, 3/16″ diameter by 3/8″ deep, is drilled into the otherwise flat-face of the rod to form a cup, which is used to hold the carbon black. The anode-cup is filled with carbon black that is tightly compacted (Alfa Aesar, 200 mesh, 99.99%). The arc is run in a helium atmosphere at a pressure of ~100 Torr and generated by a DC power-supply at 100 A. An RF component, of approximately 2 s, is used to start the discharge. In this configuration, the electron current from the cathode is carried through the rim of the anode-cup since the graphite electrode is much more conductive than the carbon black. The plasma of the arc-column extends uniformly across the entire anode surface. Optical measurements indicate the carbon black in the anode-cup is uniformly heated to a temperature of approximately 3000 °C. A typical synthesis run lasts for about 1 min, but runs performed for times ranging from 10 s to 1 min are examined. The operating conditions are optimized to minimize the erosion of the anode and the vaporization of the carbon black. After each run, the surface materials on the electrodes are analyzed using a scanning electron microscope (SEM, Hitachi S-4500).

3. Results

For a 1-min run in pure helium, a small deposit of material is formed on the cathode surface during the run. This deposit is about a millimeter in thickness and covers the entire surface of the cathode. The deposit looks similar to ones created during an arc run when two solid graphite electrodes are used. The outer edge of the deposit is hard,

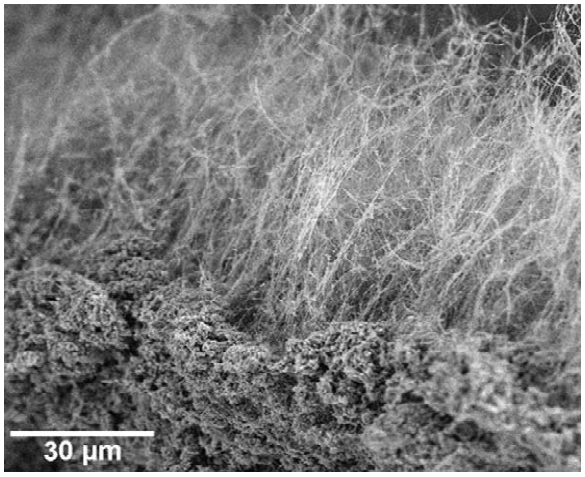

Fig. 3. Side view of MWNT layer.

brittle, shiny, and gray in color. The interior portion of the deposit contains a soft, black material, which is typically where nanotubes are found in a conventional-arc setup. At the anode, the surface is eroded several millimeters, but the erosion is not uniform. The center of the anode, which contains the carbon-black compact, is eroded more than the surrounding ROG rod. The rod itself is less eroded around its outer edge than inner cup edge. In addition, a gray-black layer, different in appearance from the original carbon black or the surrounding graphite, covers the carbon-black compact. The layer covers the entire surface of the carbon black and is about 300 μm thick. This layer can be removed, usually as a solid mat, from the surface thus exposing the darker carbon black below. No layer is formed on the portion of the anode made of solid graphite.

Scanning electron microscopy of the mat formed on the carbon black reveals that the layer is primarily composed of carbon nanotubes. Examination of the surface of the layer shows a very high concentration of nanotubes with a low concentration of other carbonaceous particles. In addition, the carbon nanotubes in the layer are long (~100 μm) and tangled with each other, as shown in Fig. 2. Looking at the nanotube layer from the side shows that the nanotubes are orientated preferentially normal to the carbon black surface and become more tangled near the upper surface of the layer (see Fig. 3). The nanotube layer is uniform in structure across its entire surface. It should be emphasized, no nanotubes are found on the graphite surface of the anode, only on the surface of the carbon black.

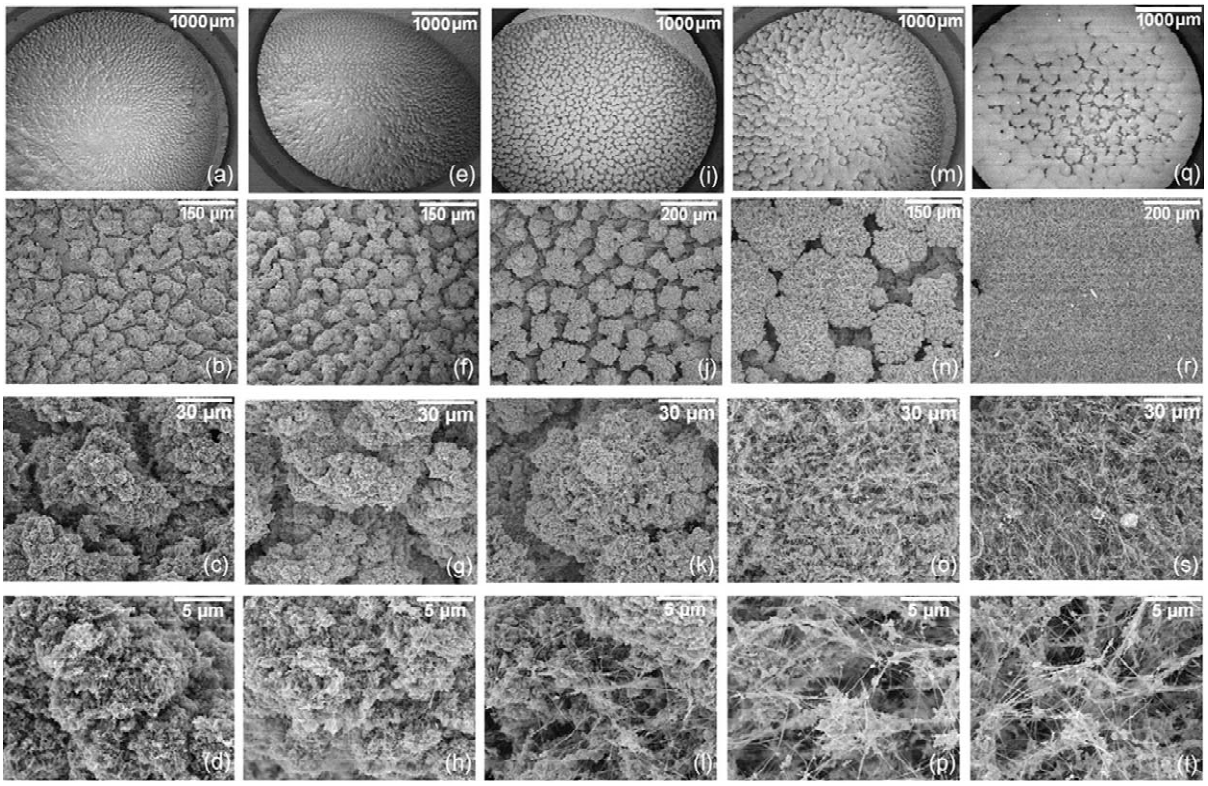

Fig. 4. Surface of carbon-black compact at different magnifications and run times: (a–d) after 10 s of synthesis; (e–h) after 20 s of synthesis; (i–l) after 30 s of synthesis; (m–p) after 40 s of synthesis; (q–t) after 50 s of synthesis.

Transmission electron microscopy of the nanotube layer reveals the structure of the nanotubes formed. The nanotubes are multiwalled nanotubes; most are composed of 20–40 walls with narrow, hollow centers. These nanotubes have smaller inner diameters and more layers than nanotubes typically grown at the cathode using a conventional-arc process. The nanotubes are near defect-free, based on the continuous lattice-fringes, and have closed ends.

To help elucidate the growth mechanism the evolution of the nanotube layer over growth time was examined. A series of experiments were run for different growth durations starting from 10 s. Fig. 4a–t are micrographs of each growth time at multiple magnifications. For runs less than 1 min, the nanotube layer does not cover the entire carbon black surface. However, the carbon black and graphite surfaces change noticeably after only 10 s. Both surfaces are eroded and the surface of the carbon black has changed in appearance. Small fissures and cracks form in the carbon black, creating small-islands domains of material on the surface, as can be seen in Fig. 4a–d. On these islands some nanotubes are already forming (see Fig. 4d). The number of nanotubes increases as the growth time is increased to 20 and 30 s and they begin to cover the tops of the islands domains, as shown in Fig. 4e–l. By 40 s, the nanotubes begin to form a continuous, tangled layer on the tops of the island domains. The island domains are also seen to grown larger and start to coalesce (see Fig. 4m–p). By 50 s, the layer of nanotubes covers most of the carbon black surface, with only a few regions of exposed carbon black remaining, as shown in Fig. 4q–t.

For growth times longer than 20 s the nanotubes are frequently observed to have one ‘free end’ that is not terminated at a support interface (see Fig. 5a). For short growth times of 10 and 20 s, when the nanotube density is low and individual nanotubes can be easily distinguished, some very interesting nanotubes are observed. Fig. 5b is a micrograph of a MWNT terminated at both ends in the carbon black. Fig. 6a is a micrograph of a Y-branched MWNT with all the ends of the Y terminated in the carbon

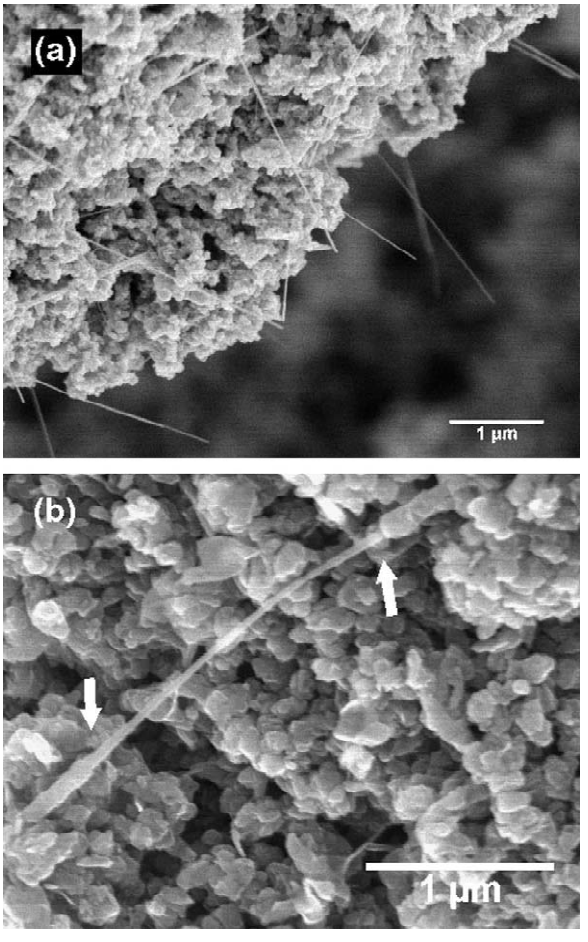

Fig. 5. (a) MWNTs with one ‘free end’ and on end terminated in carbon black. (b) MWNT terminated at both ends in carbon black.

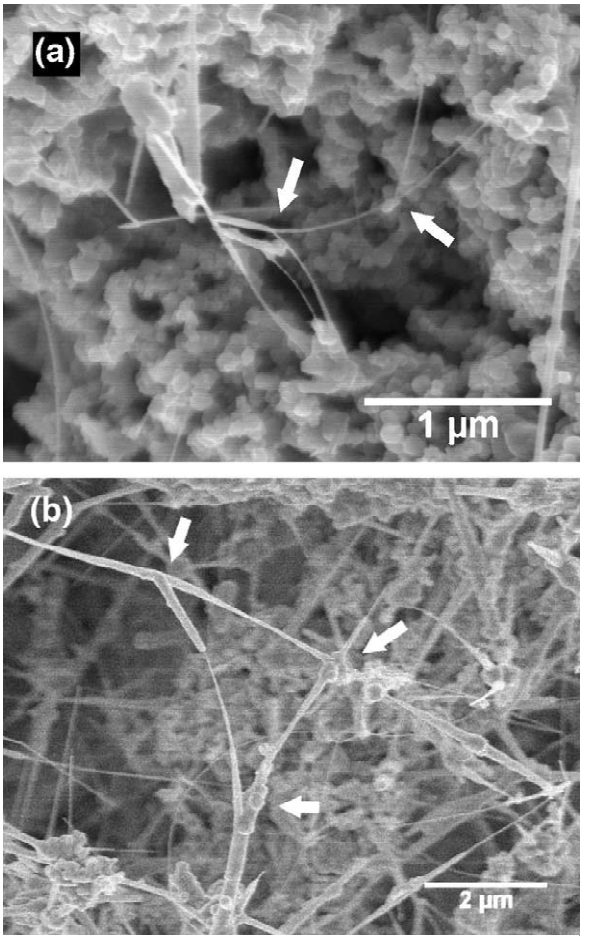

Fig. 6. (a) MWNTs with Y-branching. (b) MWNTs with Δ-branching (white arrows indicate Y-branches).

black. Fig. 6b is a micrograph of a Δ-branched MWNT. The mechanism for the growth of MWNTs from carbon black must be able to account for these features.

4. Discussion

The solid-state formation of MWNTs from carbon black can be broken into two growth stages. The basic mechanism for both stages is the same; only the origin of the tensile-force that drives the reaction differs. In the initial stage, thermally generated tensile-forces result in the formation of short nanotubes. Electrostatic forces present in the plasma of the high-temperature arc-furnace drive the subsequent extension of the short nanotubes to multiple-micron lengths.

The basic tenets of the growth mechanism are as follows: double [5–7] defects are in equilibrium with the graphene lattice, both in the carbon black and in the nanotubes, via [6–6–6–6] to [5–7–7–5] Stone–Wales switches (see Fig. 7); the [5–7] defects migrate thermally and at random, both in the carbon black and in the nanotubes, but become concentrated at locations that are energetically favorable; an energetically-favorable location is the stem of a nanotube under tensile strain; the higher concentration of [5–7] defects in the stem increases the probability of interactions between [5–7] defects that result in the self-annihilation of double [5–7] defects via a [5–7–7–5] to [6–6–6–6] reverse Stone–Wales switch; the net migration of [5–7] defects to the stem, and subsequent generation of hexagons in the stem, results in the lengthening of the stem.

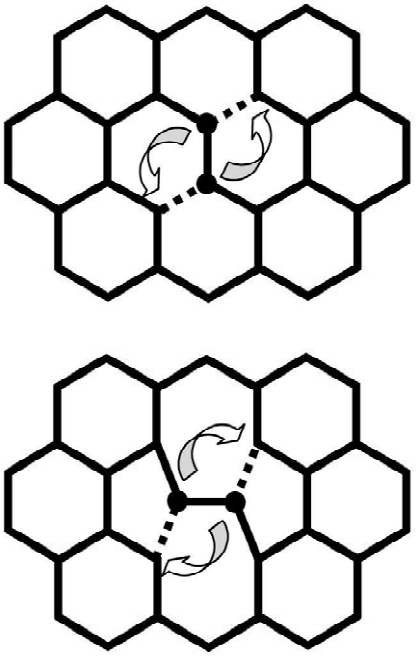

Fig. 7. Formation of a [5–7]-pair defect from four hexagons via a Stone–Wales switch and the annihilation of a [5–7]-pair defect to form four hexagons via a reverse Stone–Wales switch.

The simulated energy-of-transformation for the generation of a double [5–7] defect via the Stone–Wales bond-switch, [6–6–6–6] to [5–7–7–5] is, for all practical purposes, identical for multilayer fullerenes, 2.35 eV [43], and for nanotubes, 2.34 eV [29].[1] This would tend to indicate the [5–7–7–5] defect is neither more favored in the carbon black nor the nanotube. However, simulations also indicate the energy of formation for the [5–7–7–5] defect in the nanotube decreases with tensile stress and starts to become energetically favorable with respect to the graphene lattice at about 5% strain.

The stress necessary to produce 5% strain is large. Values of Young's modulus for MWNTs are frequently in the range of 1 TPa [44,45]. A 5% strain would, therefore, require a stress of 50 GPa. The growth mechanism, however, does not require the [5–7–7–5] defect to be energetically favorable with respect to the graphene lattice only that the [5–7–7–5] defect in the nanotube be energetically favorable with respect to the [5–7–7–5] defect in the carbon black. To lower the energy of formation in the nanotube by 0.2 eV, or ~10%, a strain of 0.5%, or stress of 5 GPa, would be needed.

A stress of 5 GPa is still quite large, particularly for an electrostatically generated force. There are, however, several factors that will tend to concentrate the stress experienced by the end of the nanotube into a smaller area within the tube stem. First, at the end of the nanotube the stress is exerted on a circular area while in the stem an annular-area undergoes the strain. Second, the annular area may not experience the stress uniformly across its entire cross-section. For MWNTs loaded in tensile-stress until failure, the breakage is described as a 'sword-in-sheath'-type facture-mechanism where a core of inner-layers pulls out from a sheath of outer-layers [46]. If the stress experienced by a particular layer of the MWNTs is time dependent and is concentrated on several layers at a time in a moving-ripple, the stress experienced by those layers could be several orders of magnitude greater than that at the nanotube tip. Third, points of negative curvature, such as occur when the tube diameter changes abruptly, can further concentrate the stress to a narrow area in the tube circumference, an example of which can be seen in Fig. 8. Fourth, for nanotubes with one 'free end', such as those in Fig. 5a, there is a local enhancement of the electric field due to the nanotube geometry.

[1] Some variations in the simulated energies of defect formation exist between authors. The energies for the defect formation cited for both the fullerene and the nanotube cited herein where generated by the Department of Physics, North Carolina State University, Raleigh, North Carolina to minimize differences introduced by different simulation methods.

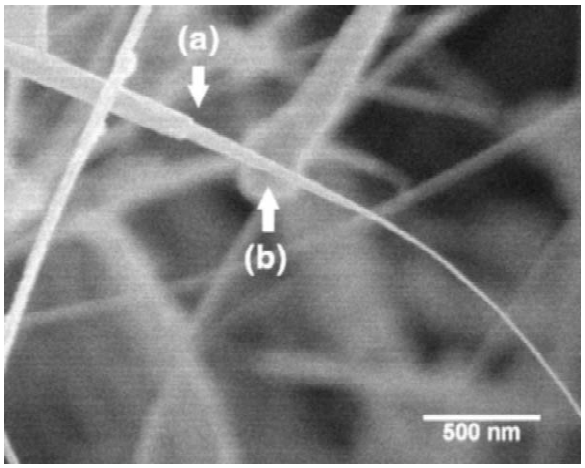

Fig. 8. Multiwalled carbon nanotube: (a) negative curvature point; (b) taper region.

The combined effects of a smaller cross-sectional area in the tube stem than at the tube end, an uneven application of the stress along the tube stem and the local enhancement of the electric field due to nanotube geometry result in stem areas where the [5–7–7–5] defect is energetically favorable with respect to the [5–7–7–5] defect in the carbon black. The defects can migrate from the carbon black and concentrate in these high stress areas of the nanotube. Because the stress is time dependent and cyclic, when the stress is removed the defects can either migrate from the nanotube area, due to their higher concentration, or undergo the reverse Stone–Wales transformation to form four hexagons. Those that undergo the reverse Stone–Wales switch add to the tube length.

A fraction of the [5–7] defects will neither undergo a reverse Stone–Wales switch nor migrate from the nanotube, but remain as defects in the tube. The lining up of [5–7] defects across multiple tube layers would lead to a taper in the nanotube, an example of which can also be seen in Fig. 8.

In the initial stage of growth thermal forces are believed to be the means by which the nanotubes are formed. Heating by the carbon arc causes coalescence and shrinkage of the carbon black. The shrinkage causes tensile stress between carbon-black particles that recede from each other. The areas of greatest stress will be at small cross-sectional area 'necks' that form at the tangential-joints between the carbon-onions that comprise the carbon black, illustrated in Fig. 9a and b. The resulting strain can be relieved in three ways; the lengthening of the neck

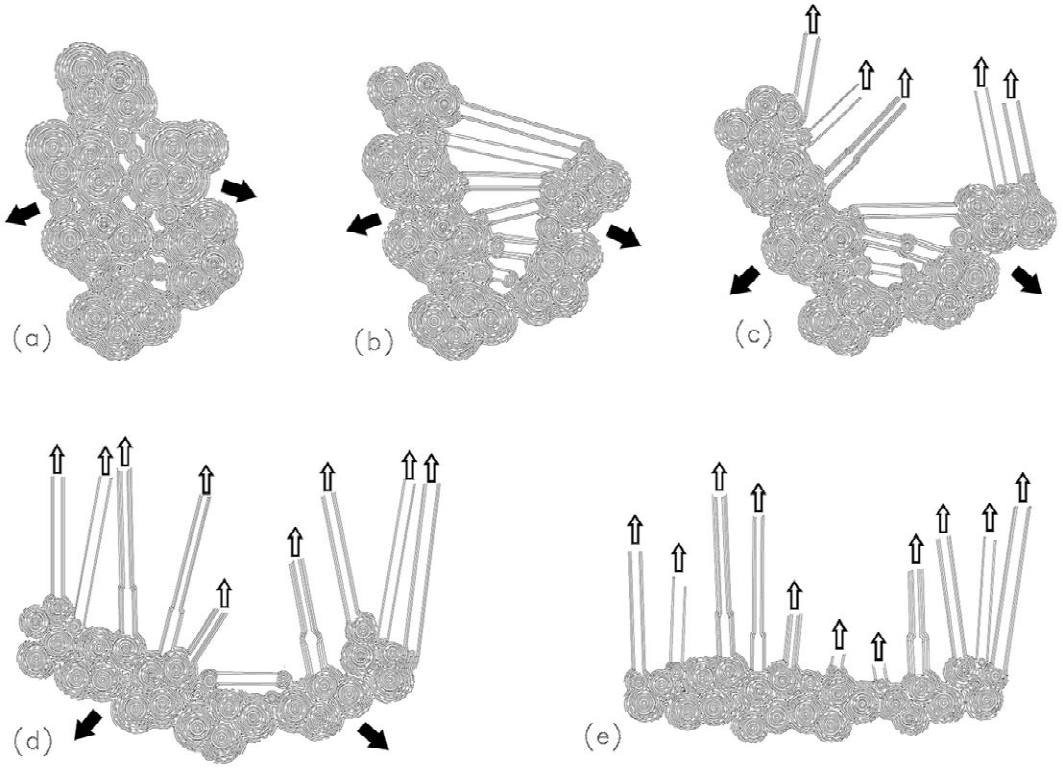

Fig. 9. Growth of MWNTs from carbon black. (a–c) Initial thermal stress stage; (d–e) electrostatic growth stage. Solid arrows (→) indicate thermal forces. Outline arrows (⇒) indicate electrostatic forces.

between the onions, the introduction of [5–7] defects into the neck, or the breaking of the neck.

The mechanism by which the neck region between onions is lengthened is the stress driven migration of [5–7] defects just outlined. During the thermal stage of growth when stress is introduced by shrinkage, no free nanotube ends, such as those in Fig. 5a are required; in fact one would expect to see nanotubes terminated at both ends in carbon black as is observed for short growth-times (10–20 s) (see Fig. 5b). During the thermal stage stresses can be along more than one axis and one might expect a Y-branching, as observed in Fig. 6a and illustrated in Fig. 10a, or even a Δ-branching, as observed in Fig. 6b and illustrated in Fig. 10b.

If the strain rate exceeds the rate at which [5–7] defects can migrate, annihilate, and lengthen the neck, one would expect the [5–7] defects to remain in the neck to provide additional strain relief. The [5–7] pairs would, however, result in the necking of the nanotube to a smaller diameter, as can be seen in Fig. 8. To this point of growth nanotubes terminated at both ends in carbon black would be expected.

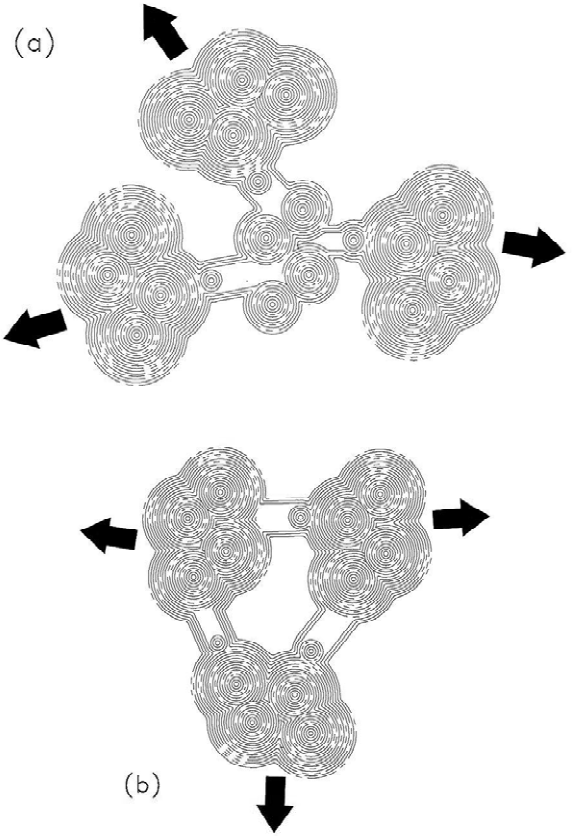

Fig. 10. (a) Growth of MWNTs with Y-branching (black arrows in insert indicate thermal forces). (b) Growth of MWNTs with Δ-branching (black arrows in insert indicate thermal forces).

When the strain rate exceeds the rate at which both hexagon formation and [5–7] defect introduction can relieve the stress, the neck will fracture, most likely at the narrowest point. If growth were terminated immediately after fracture, one would expect open-ended nanotubes. Because tube fracture occurs early in the growth cycle a large fraction of the sample is still carbon black and TEM samples are difficult to obtain. The nature of the nanotube ends at short growth-times is still under investigation. Once the neck has fractured into a tube with a free end, a mechanism for its continued growth must exist as the length of most tubes exceeds several microns. The strong electric-field present in the sheath region immediately above the anode and enhanced by the geometry of the nanotube tip provides the driving force for continued tube-growth, illustrated in Fig. 9c–e.

Both thermal and electrostatic forces are present at the plasma–anode interface and it is difficult to separate the thermal effects from the electrostatic effects. However, for growth times greater than ~40 s it is not uncommon for a continuous dense-mat of MWNTs to form over the entire surface of the carbon black. The mat can be easily removed from the bulk of the carbon black. Examination of the underside of the mat, the side not exposed to the arc plasma, can provide a first approximation of the high-temperature growth-process in the absence of an electric field and some insight into the MWNT growth-process prior to the advent of an electrostatic driving-force. Fig. 11a–c are a series of scanning electron micrographs of the underside of such a mat, grown for 50 s. The shrinkage of the carbon black into small domains, reminiscent of mud cracks in a dry river-bed, can be seen (see Fig. 11a). Typical of fractal patterns, the shrinkage patterns can be observed on a smaller scale within the large domains (see Fig. 11b). For these smaller shrinkage distances, manifold MWNTs can be seen spanning the gap between these sub-domains consistent with the proposed mechanism (see Fig. 11c).

5. Summary

A mechanism for the solid-state transformation of carbon black into MWNTs at the anode of a carbon arc has been proposed. The mechanism is divided into two stages; in the first stage the growth of short nanotubes is driven by multi-axial tensile stresses that arise from thermal shrinkage. The mechanism accounts for the presences of Y-branching and Δ-branching, as well as the large number of MWNTs terminated at both ends in carbon black for short growth times. Electrostatic forces present in the plasma of the high-temperature arc-furnace, drive the subsequent extension of the short nanotubes to multiple-micron lengths. The tendency of electrostatic forces to be along a single axis accounts for the preferential orientation of the long nanotubes along the electrode axis. For both types of

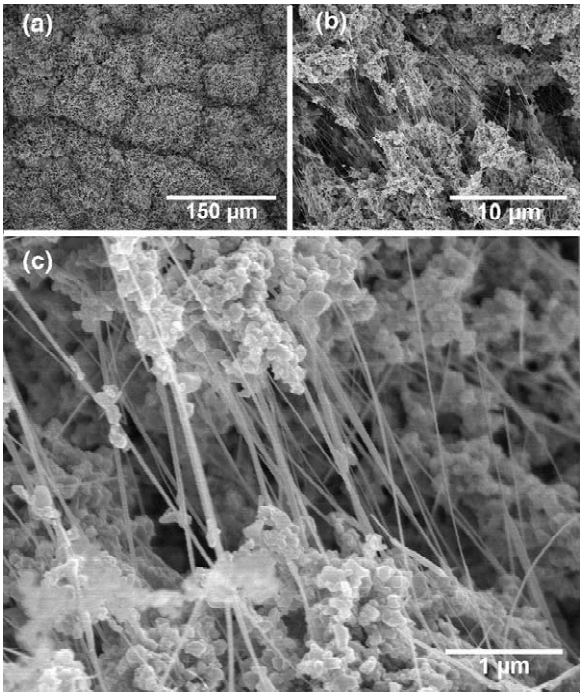

Fig. 11. Underside of carbon-black mat; side not exposed to plasma. (a) Shrinkage of carbon black into island domains. (b) Smaller scale shrinkage pattern within island domain. (c) MWNT formation across gaps in sub-domains.

growth, thermal-shrinkage driven and electrostatic-force driven, the basic growth mechanism is the same. The [5–7] defects in the graphene lattice migrate thermally to areas of high tensile strain; one such high strain area is the stem of a nanotube. The higher concentration of [5–7] defects in the stem increases the probability of interactions between [5–7] defects that result in the self-annihilation of double [5–7] defects via a [5–7–7–5] to [6–6–6–6] reverse Stone–Wales switch. The net migration of [5–7] defects to the stem, and subsequent generation of hexagons in the stem, results in the lengthening of the stem.

Acknowledgements

This project is supported by the National Science Foundation (NSF) (DMR-0071737) and the URETI program of NASA (NCC 2-1363) subcontracted through Purdue University (Agreement No. 521) at the Materials Research Institute (MRI) of Northwestern University. The use of the facilities of the Materials Research Science and Engineering Center (MERSEC) at Northwestern University supported by the NSF (DMR-0076097) is acknowledged.

References

[1] Doherty SP, Buchholz DB, Li BJ, Chang RPH. J Mater Res 2003;18(4):1.
[2] Dresselhaus MS, Dresselhaus G, Eklund PC. Science of fullerene and carbon nanotubes. San Diego: Academic Press, 1995, pp. 785–791.
[3] Ugarte D. High-temperature behavior of ‘fullerene black’. Carbon 1994;32(7):1245–8.
[4] Harris PJF, Tsang SC. High-resolution electron microscopy studies of non-graphitizing carbons. Philos Mag A 1997;7(3):667–77.
[5] de Heer WA, Ugarte D. Carbon onions produced by heat treatment of carbon soot and their relation to the 217.5 nm interstellar absorption feature. Chem Phys Lett 1993;207(4–6):480–6.
[6] Harris PJF, Tsang SC, Claridge JB, Green MLH. High-resolution electron microscopy studies of a microporous carbon produced by arc-evaporation. J Chem Soc Faraday Trans 1994;90(18):2799–802.
[7] Geohegan DB, Schittenhelm H, Fan X, Pennycook SJ, Puretzky AA, Guillorn MA et al. Condensed phase growth of single-wall carbon nanotubes from laser annealed nanoparticles. Appl Phys Lett 2001;78(21):3307–9.
[8] Sen R, Suzuki S, Kataura H, Achiba Y. Growth of single-walled carbon nanotubes from the condensed phase. Chem Phys Lett 2001;349(5–6):383–8.
[9] Maiti A, Brabec CJ, Bernholc J. Kinetics of metal-catalyzed growth of single-walled carbon nanotubes. Phys Rev B 1997;55(10):R6097–100.
[10] Gavillet J, Loiseau A, Journet C, Willamime F, Ducastelle F, Charlier CJ. Root-growth mechanism for single-wall carbon nanotubes. Phys Rev Lett 2001;87(27):2755041–4.
[11] Thrower PA. The study of defects in graphite by transmission electron microscopy. In: Walker PL, editor, Chemistry and physics of carbon, vol. 5, New York: Marcel Dekker, 1969, pp. 261–2.
[12] Krishnan A, Dujardin E, Treacy MMJ, Hugdahl J, Lynum S, Ebbesen TW. Graphitic cones and the nucleation of curved carbon surfaces. Nature 1997;388(6641):451–4.
[13] Ge MH, Sattler K. Observation of fullerene cones. Chem Phys Lett 1994;220(3–5):192–6.
[14] Dresselhaus MS, Dresselhaus G, Saito R. Physics of carbon nanotubes. Carbon 1995;33(7):883–91.
[15] Endo M, Kroto HW. Formation of carbon nanofibers. J Phys Chem 1992;96(17):6941–4.
[16] Curl RF, Smalley RE. Probing C_{60}. Science 1988;242(4881):1017–22.
[17] Iijima S, Toshinari P, Ando Y. Pentagons, heptagons and negative curvature in graphite microtubule growth. Nature 1992;356(6372):776–8.
[18] Lenosky T, Gonze X, Teter M, Elser V. Energetics of negatively curved graphitic carbon. Nature 1992;355(6358):333–5.
[19] Zhou D, Seraphin S. Complex branching in the growth of carbon nanotubes. Chem Phys Lett 1995;238(4-6):286–9.
[20] Chernozatonskii LA. Carbon nanotube connectors and planar jungle gyms. Phys Lett A 1992;172(3):173–6.
[21] Vanderbilt D, Tersoff J. Negative–curvature fullerene analog of C_{60}. Phys Rev Lett 1992;69(4):511–3.
[22] Lenosky T, Gonze X, Teter M, Elser V. Energetics of

negatively curved graphitic carbon. Nature 1992;355(6358):333–5.
[23] Charlier JC, Ebbesen TW, Lambin P. Structural and electronic properties of pentagon–heptagon pair defects in carbon nanotubes. Phys Rev B 1996;53(16):11108–13.
[24] Maiti A, Brabec CJ, Bernholc J. Structure and energetics of single and multilayer fullerene cages. Phys Rev Lett 1993;70(20):3023–6.
[25] Terrones H, Terrones M. The transformation of polyhedral particles into graphitic onions. J Phys Chem Solids 1997;58(11):1789–96.
[26] Lambin P, Meunier V. Structural properties of junctions between two carbon nanotubes. Appl Phys A 1999;68(3):263–6.
[27] Chico L, Crespi VH, Benedict LX, Louie SG, Cohen ML. Pure carbon nanoscale devices: nanotube heterojunctions. Phys Rev Lett 1996;76(6):971–4.
[28] Meunier V, Nardelli MB, Roland C, Bernholc J. Structure and electronic properties of carbon nanotube tapers. Phys Rev B 2001;64(19):1954191–6.
[29] Nardelli MB, Yakobson BI, Bernholc J. Mechanism of strain release in carbon nanotubes. Phys Rev B 1998;57(8):R4277–80.
[30] Cataldo F. The impact of a fullerene-like concept in carbon black science. Carbon 2002;40(2):157–62.
[31] Iijima S. Direct observation of the tetrahedral bonding in graphitized carbon black by high resolution electron microscopy. J Cryst Growth 1980;50(3):675–83.
[32] Zhang QL, O'Brian SC, Heath JR, Liu Y, Curl RF, Kroto HW et al. Reactivity of large carbon clusters: spheroidal carbon shells and their possible relevance to the formation and morphology of soot. J Phys Chem 1996;90(4):525–8.
[33] Kroto HW, McKay P. The formation of quasi-icosahedral spiral shell carbon particles. Nature 1988;331(6154):328–31.
[34] Donnet JB, Johnson MP, Norman DT, Wang TK. Fullerenic carbon in carbon black furnaces. Carbon 2000;38(13):1885–6.
[35] Berezkin VI. Fullerenes as nuclei of carbon black particles. Phys Solid State 2000;42(3):567–72.
[36] Setlur AA, Doherty SP, Dai YJ, Chang RPH. A promising pathway to make multiwalled carbon nanotubes. Appl Phys Lett 2000;76(21):3008–10.
[37] Bower C, Zhu W, Jin S, Zhou O. Plasma-induced alignment of carbon nanotubes. Appl Phys Lett 2000;77(6):830–2.
[38] Srivastava A, Srivastava AK, Srivastava ON. Curious aligned growth of carbon nanotubes under applied electric field. Carbon 2001;39(2):201–6.
[39] Wei Y, Xie C, Dean KA, Coll BF. Stability of carbon nanotubes under electric field studied by scanning electron microscopy. Appl Phys Lett 2001;79(27):4527–9.
[40] Wang ZL, Poncharal P, de Heer WA. Nanomeasurements of individual carbon nanotubes by in situ TEM. Pure Appl Chem 2000;72(1–2):209–19.
[41] Maiti A, Brabec CJ, Roland C, Bernholc J. Growth energetics of carbon nanotubes. Phys Rev Lett 1994;73(18):2468–71.
[42] Doherty SP, Chang RPH. Synthesis of multiwalled carbon nanotubes from carbon black. Appl Phys Lett 2002;81(13):2466–8.
[43] Brabec CJ, Maiti A, Bernholc J. Structural defects and the shape of large fullerenes. Chem Phys Lett 1994;219(5–6):473–8.
[44] Yakobson BI, Avouris P. Mechanical properties of carbon nanotubes. Top Appl Phys 2001;80:287–327.
[45] Forró L, Schönenberger C. Physical properties of multi-wall nanotubes. Top Appl Phys 2001;80:329–91.
[46] Yu MF, Lourie O, Dyer MJ, Moloni K, Kelly TF, Ruoff RS. Strength and breaking mechanism of multiwalled carbon nanotubes under tensile load. Science 2000;287(5453):637–40.